Miniature inhalation therapy platform using surface acoustic wave microfluidic atomization

Aisha Qi,[a] James R. Friend,[a] Leslie Y. Yeo,*[a] David A. V. Morton,[b] Michelle P. McIntosh[b] and Leone Spiccia[c]

Received 19th February 2009, Accepted 29th April 2009
First published as an Advance Article on the web 14th May 2009
DOI: 10.1039/b903575c

Pulmonary drug administration requires direct delivery of drug formulations into the lower pulmonary tract and alveoli of the lung in the form of inhaled particles or droplets, providing a distinct advantage over other methods for the treatment of respiratory diseases: the drug can be delivered directly to the site of inflammation, thus reducing the need for systemic exposure and the possibility of adverse effects. However, it is difficult to produce droplets of a drug solution within a narrow monodisperse size range (1–10 μm) needed for deposition in the lower pulmonary tract and alveoli. Here, we demonstrate the use of surface acoustic wave microfluidic atomization as an efficient means to generate appropriate aerosols containing a model drug, the short-acting β_2 agonist salbutamol, for the treatment of asthma. The mean aerosol diameter produced, 2.84 ± 0.14 μm, lies well within the optimum size range, confirmed by a twin-stage impinger lung model, demonstrating that approximately 70 to 80% of the drug supplied to the atomizer is deposited within the lung. Our preliminary study explores how to control the aerosol diameter and lung delivery efficiency through the surface tension, viscosity, and input power, and also indicates which factors are irrelevant—like the fluid density. Even over a modest power range of 1–1.5 W, SAW atomization provides a viable and efficient generic nebulization platform for the delivery of drugs *via* the pulmonary route for the treatment of various diseases. The control offered over the aerosol size, low power requirements, high delivery efficiency, and the miniaturization of the system together suggest the proposed platform represents an attractive alternative to current nebulizers compatible with microfluidic technologies.

I. Introduction

Inhalation therapy has become the treatment of choice for asthma and chronic obstructive pulmonary disease (COPD).[1,2] Unlike oral dosing, inhalation therapy allows a high concentration of a drug to be administered and targeted directly to local inflammation sites within the lung, thereby enabling lower total dosages, reduction in systemic side effects, and potentially hastening the onset of action of the drug.[3] Metered Dose Inhalers (MDIs) and Dry Powder Inhalers (DPIs) are commonly used for bronchodilator administration for asthma and COPD therapy; the patient inhales a pre-metered dose in a single forced inspiratory manoeuvre. There is lively debate among researchers, however, in deciding whether MDIs or DPIs are the most effective or if continuous nebulization to a patient undergoing repeated tidal breathing for a period up to several minutes is required.[4] Though the debate continues, critical factors in making such decisions are generally based on clinical judgements, taking into consideration such factors as dose level, drug efficacy and safety profile, patient age group, disease severity, ease of administration, and cost.[5]

Nebulizers are capable of delivering more drug than current MDIs and DPIs because they operate over a longer period. Moreover, nebulizers do not require coordination skills from the patient, unlike MDIs, and do not require patient actuation *via* inhalation, unlike DPIs. Nebulizers are commonly used in acute cases of COPD or severe asthma attacks where the patient is unable to self-medicate.[6] For this same reason, nebulizers may be more appropriate for paediatric and geriatric patient populations.

Historically, nebulizers have been large, cumbersome, less portable and more expensive than MDIs or DPIs. Furthermore, conventional nebulizers generally have low dose efficiencies; although more drug may be delivered into an aerosol, much of the aerosolized drug is subsequently wasted[7,8] because

1. aerosols are generated continuously, wasting drug as the patient exhales against the nebulizer's output,

2. the aerosols have polydisperse size distributions, with a significant fraction of droplets too large for deep lung deposition, and since

3. nebulizers typically have a large internal residual volume.

For inhalation therapy to be most effective, the droplet's aerodynamic behaviour (governed by Stokes' law) is of fundamental importance.[9] For deep lung deposition, an aerodynamic diameter less than 5 μm or preferably 3 μm is considered appropriate, such that the aerosol can avoid inertial impaction in the oropharyngeal region. For deposition higher up in the airways, a larger aerodynamic diameter may be preferred.[2,10–12] As a result, the aerosol droplet size is crucial to the efficacy of

[a]*Micro/Nanophysics Research Laboratory, Monash University, Clayton, VIC, 3800, Australia. E-mail: leslie.yeo@eng.monash.edu.au*
[b]*Monash Institute of Pharmaceutical Sciences, Monash University, 381 Royal Parade, Parkville, VIC, 3052, Australia*
[c]*Department of Chemistry, Monash University, Clayton, VIC, 3800, Australia*

inhalation therapy, and therefore an ideal device capable of efficiently delivering high doses of a drug would permit precise control of the droplet size distribution and preferably offer large atomization rates to deliver the desired dosage in as short a time period as possible to minimize patient distress and inconvenience.

Nebulization technology has rapidly progressed in recent years, with new methods that utilize ultrasound[8] and electrohydrodynamic atomization,[13–15] allowing greater control over the atomization process to provide aerosols with reduced spreads of polydispersity and with droplet size tuning capability. Moreover, these methods can be incorporated into micro-electro-mechanical-systems (MEMS) and microfluidic chips, offering an attractive alternative to the large and cumbersome nebulizers that are currently available commercially.[16,17] Unfortunately, there are inherent limitations associated with such devices. For example, MEMS devices are plagued with reliability issues associated with wear and tear as a consequence of friction and stiction at small scales. Electrohydrodynamic atomization is restricted to high voltage operation—typically several kilovolts—raising safety and reliability issues in consumer use. Various types of ultrasonic atomization have been devised over the years, and the most common systems use a bath of liquid from which a piezoelectric disc generates an aerosol plume. These ultrasonic nebulizers are also relatively large in size, have limitations on output and size control, and often precipitate the solubilized drug onto the atomization reservoir walls due to solvent evaporation,[8] wasting the drug and requiring regular cleaning by the user. More recent designs using meshes for nebulization offer better portability, dosage rates, and aerosol monodispersity.[18,19] The mesh has chemically or laser-cut microscopic holes, forming thousands of orifices that generate droplets under irradiation by ultrasound, although these meshes are prone to clogging, which significantly reduces throughput. In the context of these past and current technologies, a small, portable, reliable, and relatively cost-effective device remains out of reach, especially one that can effectively generate non-agglomerating droplet size distributions which are suitably monodisperse and less than 5–10 μm in diameter.

In this paper, we propose the use of a promising alternative to ultrasonic nebulization based on surface acoustic wave (SAW) atomization.[20–24] Surface acoustic waves are MHz to GHz-order, transverse-axial polarized elliptical electroacoustic waves with displacement amplitudes of just a few nanometers. Here, they are generated on and traverse the surface along the x-axis of 127.86° y–x rotated single-crystal lithium niobate ($LiNbO_3$) which is a low-loss piezoelectric material. Unlike typical ultrasound, which is a bulk phenomenon, the SAW is confined close to the substrate surface, its amplitude decaying rapidly over a depth of four to five wavelengths (several hundred microns) into the substrate material. Compared to conventional ultrasonic atomizers that consume power on the order of 10 W, SAW atomizers therefore only consume between 0.5–3 W since most of the energy is contained within a localized region close to the surface of the substrate and hence can be transmitted into the fluid much more efficiently than ultrasound. Moreover, the customized SAW device and its driver in this study (requiring only two CR123 lithium cell batteries) are both small as shown in Fig. 1, illustrating the potential of the device for portable applications,

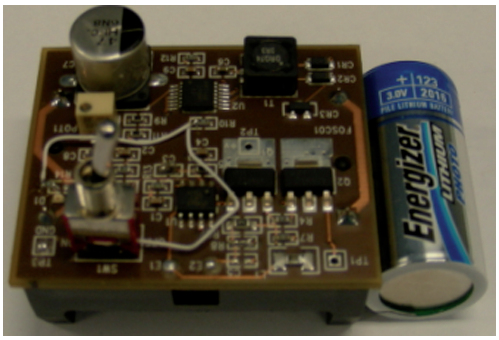

Fig. 1 Image of a small driving circuit fabricated as a power source for the SAW atomizer. It uses two CR123 lithium cell batteries, such as that shown on the right hand of the circuit. The maximum output of this driving circuit is about 30 V_{p-p}.

most recently for lab-on-a-chip synthetic chemistry.[25] Moreover the 10–100 MHz order frequency employed in SAW devices, significantly higher than the 10 kHz–1 MHz frequency range of typical ultrasonic devices, induce vibrations with a period much shorter than the molecular relaxation time scale associated with large molecules in liquids,[26] and thus the risk of denaturing molecules or lysing cells is greatly reduced. Further, as the frequency is increased, the power required to induce cavitation increases far beyond what is needed for atomization, eliminating the effect of cavitation-induced lysis or shear in SAW atomizers.[20]

Our aim is to investigate the use of SAW atomization to generate aerosols which approach a narrow size distribution of a model drug, namely, the short-acting β_2 agonist salbutamol ($C_{13}H_{21}NO_3$), within a 1–5 μm size range that is optimal for inhalation therapy.[12,27] In choosing this model drug, we aim to demonstrate the feasibility of SAW atomization as a delivery platform for the treatment of asthmatic patients, although the technology constitutes a generic platform for pulmonary delivery of a wider range of aerosolized drugs in a form compatible with microfluidic lab-on-a-chip technologies. In particular, we restrict our focus to measurements of the aerodynamic size distribution of the generated aerosols and demonstrate that the near-optimal size distributions attained will lead to high lung deposition efficiency in the target area.

The rest of this paper is organized as follows. Section II describes the experiments employed in this project. Specifically, we begin with a description of the SAW, how it is generated, and how it gives rise to the atomization of a liquid. Subsequently, we provide details on the model drug formulation followed by a description of the tools and methods employed to characterize the aerosol. The results are then presented in Sec. III. In particular, we discuss the aerosol size distributions obtained using laser diffraction techniques in Sec. IIC. This is followed by high-speed flow visualization studies to elucidate the dynamics associated with the atomization process. It is hoped that these studies will provide an understanding of why the specific droplet sizes arise and how they can be controlled. With the aid of a twin-stage impinger lung model, we then discuss the effects of the system parameters—for example, the applied power and the solvent concentration—on the lung dose in Sec. IIIC. Finally, we provide concluding remarks in Sec. IV.

II. Materials and methods

A. Surface acoustic wave device

An illustration of this SAW device is shown in Fig. 2(a). A pair of aluminium–chromium interdigital transducers (IDTs; see Fig. 2(b)) was fabricated using sputtering (Hummer® Triple-target Magnetron Sputter System, Anatech, USA.) and standard UV photolithography with wet etch techniques onto a 128° *y*-cut *x*-propagating lithium niobate ($LiNbO_3$) piezoelectric substrate surface. Details of the fabrication procedures can be found elsewhere.[28,29] A high frequency electrical signal is supplied to the IDT electrodes, generating mechanical oscillations on the substrate *via* the inverse piezoelectric effect, thereby producing a *Rayleigh wave* SAW, as shown in Fig. 2(c), that propagates along the surface of the substrate in both the positive and negative *x*-axis directions from the IDT. For this simple IDT configuration, the gap and width of the IDT fingers are set to be a quarter of the SAW wavelength λ_{SAW}, as illustrated in the inset of Fig. 2(a). The resonant frequency of the SAW device is then given by $f = c_s/\lambda_{SAW}$, where c_s is the Rayleigh SAW sound speed in the substrate. In this case, we pattern the IDT fingers to give $\lambda_{SAW} = 200$ μm such that $f = 20$ MHz since $c_s = 3965$ m s^{-1}.

A nozzle just above the surface of the substrate supplies a controlled delivery of fluid in the form of a drop on the surface. A syringe pump (Model 789100, KD Scientific, USA) is employed to regulate the amount of liquid fed to the substrate. In our experiments, we adjusted the flow rate on the syringe pump to maintain a constant volume (≈ 4 μl) of liquid on the SAW device. In this case, the atomization rate is approximately equal to the flow rate of liquid supplied by the syringe pump. In liquid media, bulk sound waves travel much slower than the Rayleigh SAW. For water, the sound speed is $c_l = 1485$ m s^{-1}, less than half $c_s = 3965$ m s^{-1}. The SAW will refract upon coming into contact with the fluid, as shown in Fig. 2(c). The angle (with respect to the vertical axis) at which the wave refracts into the liquid is given by the ratio of the sound speeds in both media, *i.e.*, $\theta_R = \sin^{-1}(c_l/c_s)$, and is known as the *Rayleigh angle*. Concomitant with the wave refraction is a leakage of acoustic energy into the liquid drop. With sufficient power, the acoustic wave in the liquid causes compression waves in addition to the displacement waves; together they are responsible for driving a strong inertial recirculation within the drop known as *acoustic streaming*.[28–31] The angle at which the wave refracts into the fluid also gives rise to a horizontal body force component on the drop, causing it to translate along the substrate.[29] The vertical acceleration of the substrate, on the other hand, gives rise to capillary wave vibrations along the free surface of the liquid drop.

Though the displacement of the substrate is only about 10 nm when applying about 100 mW of power to the SAW device, it occurs at 20 MHz, thus generating accelerations on the order of 10^9 m s^{-2}. Capillary waves appear on the free surface and quickly grow to become unstable, leading to the formation of tiny jets emanating from the free surface that subsequently break up to form atomized aerosol droplets.[20] In this work, we employ a combination of SAW-driven drop translation and atomization to produce aerosols of controlled dispersity and size for delivering the drug.

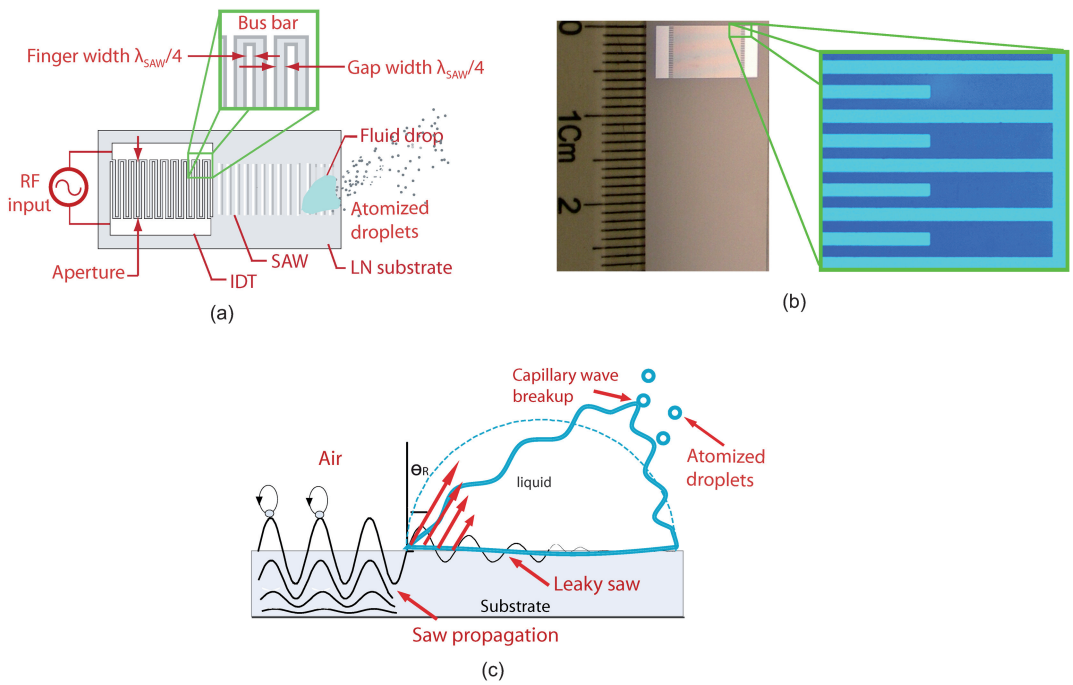

Fig. 2 (a) Schematic of the SAW device showing the IDT electrodes patterned on the piezoelectric ($LiNbO_3$) substrate. A RF power source supplies the atomizer with a sinusoidal electric signal *via* the IDT which excites the SAW on the substrate. (b) Image of the SAW substrate showing an enlargement of the IDTs for a 20 MHz SAW device. (c) Interaction of the SAW with a liquid drop placed on the substrate as shown in image (a). The SAW energy leaks into the drop and induces capillary waves on its free surface. Due to the large energy transfer, the interface rapidly destabilizes and results in the atomization of the drop through break-up of the capillary waves.

B. Model drug system

The purpose of this work is to demonstrate the potential benefits of employing a SAW atomization device as a generic nebulization platform for the pulmonary delivery of drugs for the treatment of a variety of conditions. As such, we have chosen a short-acting β_2 agonist used in the treatment of asthma as an exemplar of the platform's potential: salbutamol $C_{13}H_{21}NO_3$ (Sigma-Aldrich, Australia). Since salbutamol is not water-soluble, yet freely dissolves in alcohol, we employ a mixture of ethanol and octanol as solvents in this study. Given that this work is a preliminary investigation of a model system, the toxicological aspects of these solvents are not considered in detail. However, we note that octanol has been considered for use in the lung in addressing ataractic effects,[32] in treating acute pulmonary edema,[33,34] and has further been reported to be a promising pulmonary treatment, in combination with other drugs, for lung related diseases.[35]

Furthermore, the choice of ethanol and octanol helps avoid issues with precipitation; even though salbutamol sulfate, which freely dissolves in water, is another common form of a short-acting β_2 agonist used in the treatment of asthma, the evaporation of water causes the drug to precipitate onto the atomizer surface during atomization. Moreover, the higher surface tension and lower viscosity of water, compared to either ethanol or octanol, lead to the generation of aerosol with larger diameters D, as suggested from our previous work on SAW atomization:[20]

$$D \sim \frac{\gamma H^2}{\mu f L^2} \tag{1}$$

where γ and μ are the surface tension and viscosity of the liquid, respectively, and H and L are the characteristic height and length scales of the parent drop. A more specific discussion on this theory will be given in Sec. IIIA. We note here, however, that although it is physically intuitive that inertia would play a significant role in eqn (1), especially given the large surface accelerations generated as the SAW traverses the substrate, as alluded to earlier in Sec. IIA, it has been demonstrated that such inertial stresses are largely confined within a thin boundary layer directly adjacent to the substrate of thickness[20]

$$\delta \sim \left(\frac{\mu}{2\pi\rho f}\right)^{1/2} \sim 10^{-7}\ \mathrm{m} \tag{2}$$

where ρ is the fluid density. Away from this boundary layer in the bulk of the parent drop, viscous dissipation gives rise to fluid streaming within the drop. Whilst the size of the atomized droplets therefore depends on the capillary instability wavelength arising from the capillary–viscous force balance in eqn (1), the instability threshold at the onset of atomization however depends on an acoustic capillary number which involves a competition between the destabilizing inertial forces arising due to the acoustic forcing and the stabilizing capillary forces.[20]

Regardless, we have chosen the salbutamol/ethanol/octanol system as a model excipient/solvent system to simply demonstrate the preliminary feasibility of the device for inhalation therapy. We consider ethanol : octanol solvent concentrations ratios of 20 : 80, 50 : 50, 80 : 20 and 0 : 100 while maintaining a fixed salbutamol concentration of 0.5 mg ml^{-1} so that the effect of the working solution's surface tension and viscosity on the efficacy of the dose delivery may be determined. Octanol has a similar surface tension to ethanol, approximately 27.1 and 21.97 mN m^{-1}, respectively, but a viscosity (7.288 mPa s) roughly seven times larger than ethanol's (1.074 mPa s).

C. Aerosol characterization

The aerosol size distributions were measured using laser diffraction (Spraytec, Malvern Instruments, UK) with a range of droplet sizes between 0.1 and 2000 μm, covering the desired 1–10 μm range. Five parameters were chosen to characterize the aerosol size distribution for the salbutamol/octanol system, D_{v10}, D_{v50}, D_{v90}, D_{32} and D_{43}. The former three parameters represent the volume equivalent diameter for which 10%, 50% and 90% of the aerosol droplets fall below, respectively. These volume-based particle size distributions are equivalent to weight distributions when the particles are droplets of unit density and constitute a convenient means for comparison since it provides a direct estimate of the delivered drug mass or dose.[12,36] The parameters D_{32} and D_{43}, namely the Sauter (surface area moment) and De Brouckere (volume moment) mean diameters, respectively, are average particle sizes relevant to the dose's delivery efficiency. The data recorded represent the physical diameters of the droplets and are converted into equivalent aerodynamic diameters using the following relationship:

$$D_a = \left(\frac{\rho}{\rho_0}\right)^{1/2} D \tag{3}$$

D_a and D are the aerodynamic and the physically measured diameters, respectively, while ρ is the density of the droplet and $\rho_0 \equiv 1$ g cm^{-3}. The aerodynamic diameter is therefore equivalent to the diameter of a sphere with unit density ρ_0 that behaves in a manner that is *aerodynamically* equivalent to the droplet, *i.e.*, both the droplet and the sphere of unit density have the same terminal sedimentation velocity U.[12] At the steady-state terminal velocity, the Stokes drag μUD therefore balances the gravitational force $\rho D^3 g$, g being the gravitational acceleration, and hence the $D \sim \rho^{-1/2}$ scaling observed.

The aerosol concentration, defined as the number of aerosol droplets produced from the parent drop in each second per cubic centimeter of air, was also measured as a function of time using a Condensation Particle Counter (Model 3775, TSI Inc., USA), which has an upper limit of 10^7 particles cm^{-3} s^{-1}. In order to keep the number of atomized aerosols below this threshold, the input power to the SAW device for these experiments was limited to approximately 1 W. Each set of atomization experiments was repeated three times to ensure repeatability and reliability in the measurements. In addition, the atomization was visualized using a high-speed camera (Mikrotron, Germany) capable of a maximum record rate of 3047 frames s^{-1}, connected to a long distance microscopic lens (Infinity, USA) to examine the free surface of the drop during atomization as it destabilizes. The purpose of the visualization was to provide data on the droplet formation dynamics to aid our modelling and interpretation.

D. Lung model

A glass single cut-point twin-stage impinger (see Fig. 3[37]) was employed as an *in-vitro* model of the human pulmonary system in

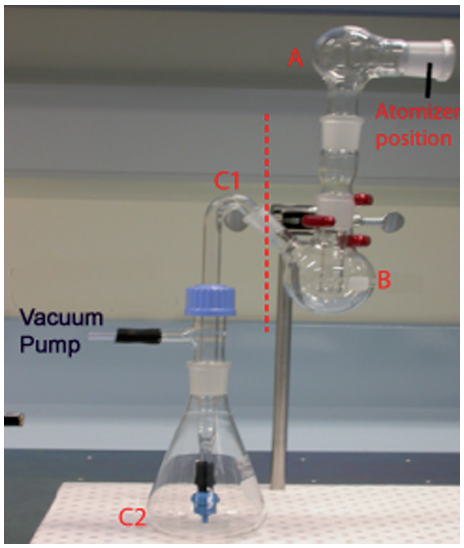

Fig. 3 Image of the glass twin-stage impinger lung model employed for the dose measurements. A vacuum pump was connected to the impinger at the marked position to simulate the inhaled air flow. The SAW atomizer is placed at the entrance of the impinger, which constitutes the 'mouth' and oral cavity (region A). Region B represents the pharynx and larynx of the upper respiratory tract, and region C, which can be further subdivided into subregions C1 and C2, is a model of the lower respiratory tract including the bronchi and the entire targeted lung area.

accordance with accepted pharmaceutical standards.[38] The impinger stages were filled with ethanol to collect and dissolve the salbutamol–octanol aerosols, and an airflow of 60 l min^{-1} was drawn through the impinger during aerosol generation, as shown in Fig. 3. At this flow rate, it is estimated that droplets with aerodynamic diameters greater than 5.8 μm are deposited in stage 1, representing the upper respiratory airway walls[39]—regions A and B—due to the dominance of inertia in their motion.[12] Droplets with aerodynamic diameters less than 5.8 μm deposit in the lower respiratory airways, *i.e.*, stage 2, which is represented by subregions C1 and C2, due to either diffusion-driven molecular collision with lung tissue or gravitational sedimentation.[12]

The *theoretical dose* is the total volume of the drug solution delivered to the SAW device, while the volume actually atomized from the SAW device is defined as the *emitted dose*. Droplets that deposit in region A form the *mouth dose*, and the droplets that remain to eventually be deposited in subregions C1 and C2 constitute the *lung dose*. The emitted dose and the lung dose are therefore the two most important values in this study, not only because they are the criteria by which the efficiency of the drug delivery atomizer is judged, but also—and more importantly—they indicate the potential of the device for pulmonary drug administration in a clinical setting. Formally, the emitted dose is defined as the amount of drug solution that is not only atomized but also permanently leaves the atomizer. Large droplets atomized from the device that fall back onto the parent drop due to their large mass are therefore omitted from this value; the emitted dose is therefore the theoretical dose minus the drug lost on the SAW atomizer. The lung dose, in contrast, represents the quantity of the drug particles that is transported to the target lung area and would subsequently provide a pharmacological effect.[9]

The lung fraction in our experiments is determined by comparing the lung dose, *i.e.*, the concentration of salbutamol in region C with the theoretical dose delivered to the atomizer. The salbutamol concentration and hence dose is measured using UV spectrophotometry (Cary 300 UV-Vis Spectrophotometer, Varian Inc., USA). Fig. 4(a) shows the UV absorption of standard salbutamol solutions that we employ as calibration curves. Salbutamol absorbs UV light at 224 and 278 nm, and the UV absorption of salbutamol varies linearly with respect to the concentration of salbutamol at each of these wavelengths, as shown in Fig. 4(b). The salbutamol concentration in each region in the glass impinger can then be obtained by comparing the measured UV absorption against both these calibration curves; having two different calibration curves permits validation of the UV absorption data of the testing samples. However, at very low concentrations (<0.01 mg ml^{-1}), the UV absorption of salbutamol at 224 nm provides a more accurate estimate, while UV absorption at 276 nm is more reliable at higher concentrations (>0.2 mg ml^{-1}).

III. Results and discussion

A. Aerosol size distribution

Fig. 5(a) shows the aerosol size and cumulative size distributions for the salbutamol/octanol system. The former is a bimodal distribution with peaks around 3.95 and 244.4 μm. The high-speed flow visualization experiments provide insight to help explain this result. Fig. 6 shows that as the power is increased, there is an increasing tendency for the parent drop to deform into a sharp axisymmetric cone that leans at the Rayleigh angle, as illustrated in Fig. 2(c) and evident in the first panel of Fig. 6(c) in which large amplitude, long wavelength (on the order λ_{SAW}) capillary undulations that propagate across the free surface of the parent drop can be clearly seen. Such deformation generally has two effects on the size of the atomized droplets.

A dominant force balance between the capillary and viscous stresses suggests the scaling relationship in eqn (1) for the diameter of the droplets ejected off the free surface due to capillary jetting and break up.[20] Equation (1) then suggests a shift towards smaller aerosol droplets as the aspect ratio of the parent drop H/L decreases, *i.e.*, as the drop spreads into a film. A liquid thin film is also easier to atomize than a liquid drop since less energy is lost due to viscous damping;[20] atomization rates will be discussed subsequently in the context of solvent effects in Sec. IIIB. The ease of atomization is evident in Fig. 6. At low input powers, the drop does not deform into an axisymmetric cone and, instead, due to the hydrophilicity of the substrate, spreads out over a relatively large area along the substrate as shown in Fig. 6(a). The small aspect ratio then results in atomization to form smaller 1 μm order droplets, which can be seen as the mist in Fig. 6(a). As the power input is increased, however, the parent drop no longer spreads out but deforms into the axisymmetric conical shape, leading again towards atomization to form larger 10–100 μm order droplets, as shown in Fig. 6(b) and 6(c). Because of the quadratic dependence of the ejected droplet diameter on the drop aspect ratio H/L in eqn (1), a small change in the aspect ratio will cause a large change in the size of droplets atomized from the surface. Thus, it is clear that increasing the

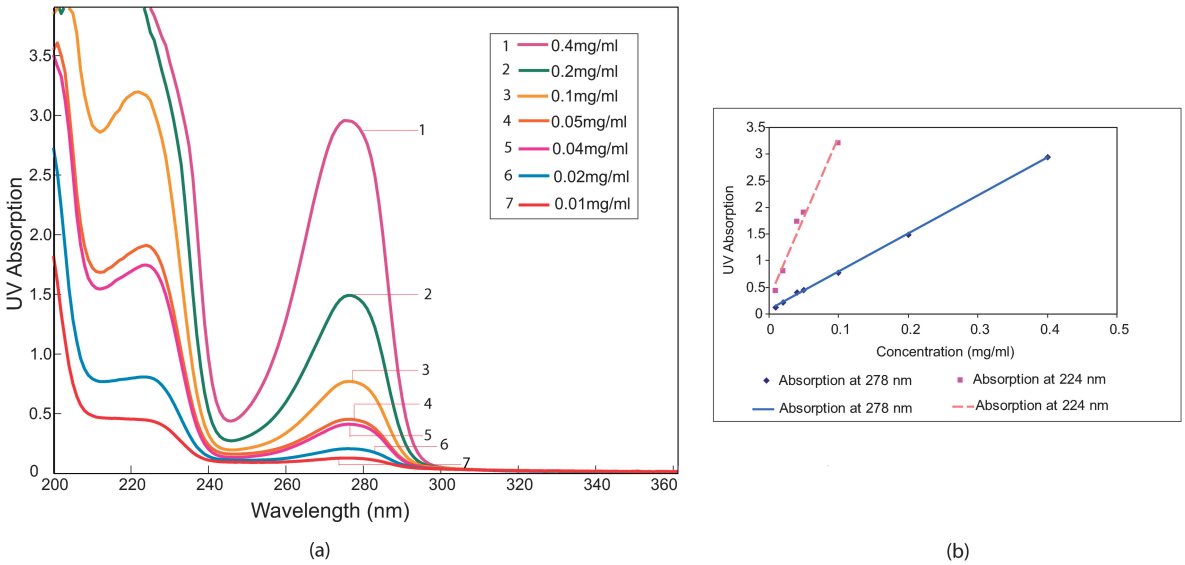

Fig. 4 (a) UV absorption peaks for solutions with different salbutamol/ethanol concentrations, obtained using UV-Vis spectrophotometry. Two absorption peaks are evident, at around 224 and 276 nm. (b) Calibration curves based on the absorption peaks obtained in (a) used for the dose measurements from the different regions in the lung model.

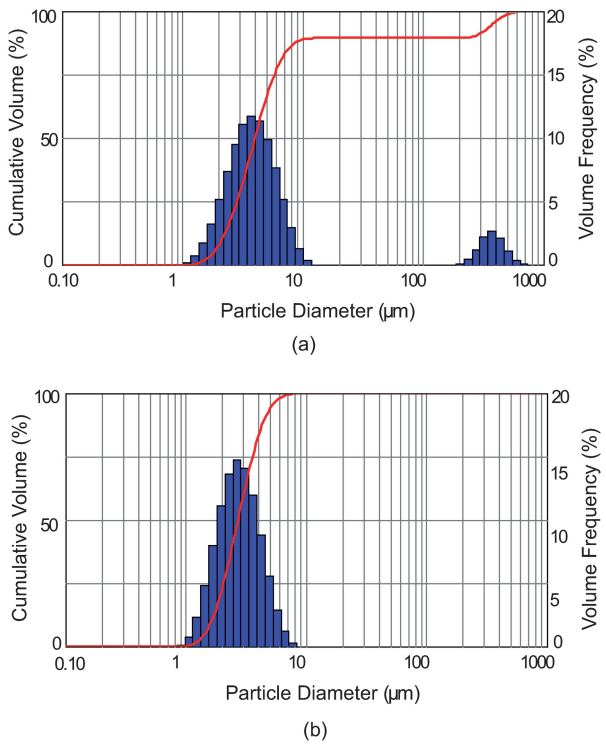

Fig. 5 Volume-based droplet size (column) and cumulative size (solid curve) distribution obtained from the atomization of salbutamol/octanol at 1.5 W, measured by laser diffraction. (a) Droplet sizes from the original experiments show a bimodal distribution with peaks at 3.95 and 244 μm. The large 100 μm order peak probably appears due to whipping of the crest off the tip of the parent drop which has axisymmetrically deformed into a conical shape.[20] (b) Droplet sizes after suppression or removal of the larger droplets indicate a narrow monodisperse distribution with $D_{v50} = 2.84 \pm 0.14$ μm and $D_{v90} = 4.55 \pm 0.20$ μm.

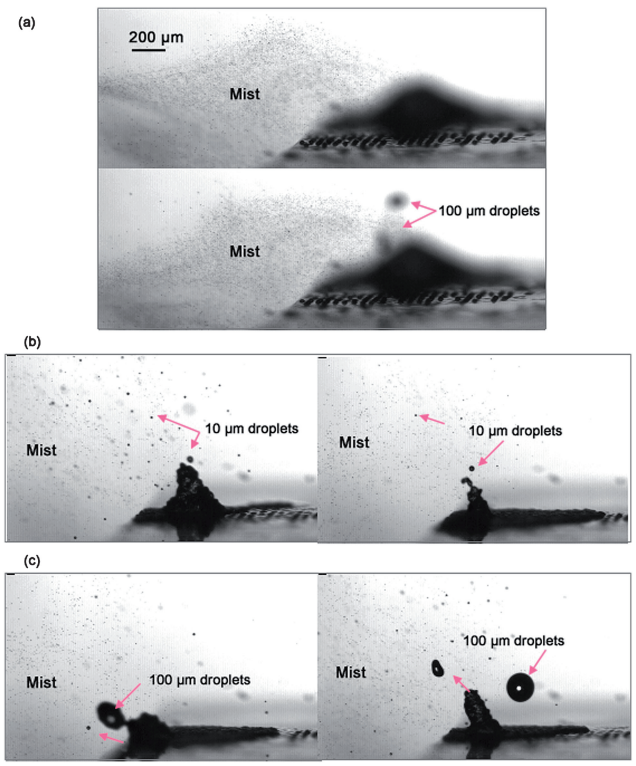

Fig. 6 High-speed flow visualization of the atomization of the salbutamol/octanol system with an applied power of (a) 1.5 W showing the generation of a mist of 1 μm order droplets, (b) 2.2 W showing the generation of larger 10 μm order droplets in addition to the 1 μm order droplet mist, and, (c) 2.8 W showing the generation of large 100 μm droplets. The SAW is propagating from the right to left in these images.

power increases the average droplet size, as well as the dispersity of the size distribution. The standard deviation of droplet diameters can increase from less than 0.5 to more than 100 when the power goes from a low of 1.5 W to a high of 3 W. Therefore, choosing a low power is beneficial for both reducing the droplet size and the polydispersity of the droplets.

A second mechanism can also give rise to the formation of droplets larger than 100 μm.[20] The large amplitude, long wavelength (on the order λ_{SAW}) capillary undulations that propagate across the free surface of the deformed conical parent drop, evident in the first panel Fig. 6(c), can cause the crest of the drop to whip and pinch off to form a large droplet,[20] as shown in the image sequence in the subsequent panels in Fig. 6(c). Due to their large mass, the large 100 μm droplets would be too heavy to be transported by the airflow into the respiratory tract, and either fall back onto the parent drop, or deposit within the oral cavity. Suppression of these larger 100 μm order droplets would clearly be beneficial to prevent wastage. The insights from the high-speed flow visualization studies reveal that this is possible by limiting the power consumption to 1.5 W, thus allowing atomization to occur from a relatively thin film, forming a dense, monodisperse droplet mist from the parent drop. Moreover, the clear separation between the two peaks in Fig. 5(a) also indicates that undesirable droplets above 100 μm can be filtered out using a form of impaction plate baffle, similar to the type usually employed in jet nebulizers.[8] A narrow monodisperse aerosol mist can then be reliably obtained as shown in Fig. 5(b).

Under these conditions, mists were sized using laser diffraction, as described in Sec. IIC. The aerodynamic diameter of the mist droplets were estimated to be equal to the product of the droplets' physical diameter and the factor $0.824^{1/2}$, where 0.824 g cm^{-3} is the density of octanol, as suggested by eqn (3). The results are summarized in Table 1.

Several workers have shown that impaction in the upper airways is governed by Stokes law, as noted above, which means that for efficient deep lung delivery, droplets below 5 μm are desired. The Stokes impaction parameter (D^2V) suggests a more crucial dependence on the aerosol diameter given its squared dependence as compared to the aerosol velocity upon impact V.[12] Our results are therefore encouraging—90% of the total volume of aerosol produced has an aerodynamic diameter below 4.55 ± 0.20 μm. Consequently, much of the drug is anticipated to be transported to the deep in the lung even if the patient is breathing rapidly. Nevertheless, this result will be verified in Sec. IIIC through the use of a lung model which reveals the percentage of droplets deposited in the various lung regions.

B. Effect of solvents

Fig. 7 plots the Condensation Particle Counter data for different octanol/ethanol solvent ratios. As the ethanol concentration is increased, the number of aerosol droplets generated through the SAW atomization process sharply decreases. Recalling that the surface tension of octanol and ethanol are similar, but that the viscosity of octanol is roughly seven times higher than ethanol, eqn (1) predicts that the greater the ethanol concentration, the larger the ejected droplets produced. Although the Condensation Particle Counter does not discriminate the droplet counts based on size, we generally observe the number of droplets to decrease as their size increases. This can be confirmed by the images in Fig. 8 in which we observe that the salbutamol/ethanol system produces larger but fewer droplets whereas the salbutamol/octanol system produces smaller but a significantly greater number of droplets, as observed by the mist above the parent drop. By adjusting the properties of the fluid's viscosity, the aerosol size may therefore be controlled.

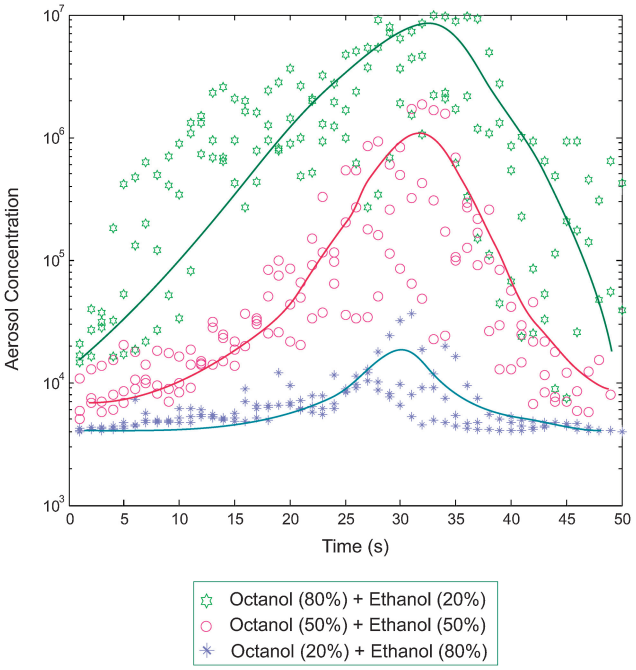

Fig. 7 Aerosol number concentration over time for different solvent (octanol/ethanol) concentration ratios measured using a Condensation Particle Counter. The atomization is carried out at a power of 1.5 W. The baseline concentration of 4×10^3 is attributed to the presence of dust particles in the ambient medium. The trendlines are included to aid visualization.

There is another physical effect on the atomization evident that is not captured by our theory: the volatility of the solvent. While the curves in Fig. 7 show that the atomization rate reaches a maximum around 30 s after power is applied to the SAW device regardless of the relative amounts of octanol and ethanol that make up the solvent, we observe little atomization in the first 20 s for solutions dominated by ethanol. Note that the baseline value

Table 1 Standard values of the aerosol aerodynamic size ($n = 4$)

	D_{v10}/μm	D_{v50}/μm	D_{v90}/μm	D_{32}/μm	D_{43}/μm
Mean	1.78 ± 0.09	2.84 ± 0.14	4.55 ± 0.20	2.65 ± 0.13	3.23 ± 0.22
Max	2.95	4.32	6.61	4.12	9.04
Min	0.72	1.53	2.64	1.40	1.68

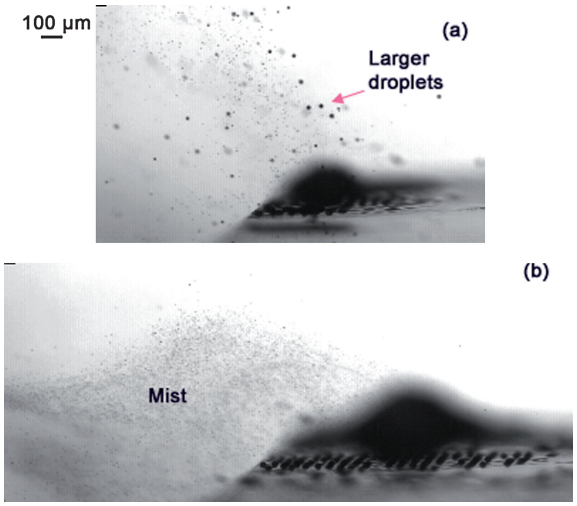

Fig. 8 Images of the atomization process of salbutamol dissolved in (a) ethanol, and (b) octanol, captured using high-speed flow visualization. Note the generation of large 10 μm droplets in the salbutamol/ethanol system which is notably absent for the salbutamol/octanol system. The input power is 1.5 W and the SAW is again propagating from right to left in the image.

of 4×10^3 is typically associated with the number of dust particles suspended in the ambient environment. Observation of the parent drop in this initial transient (not shown) reveals that during this time, considerable evaporation of the ethanol occurred—the loss in volume thus resulted in considerable retraction of the drop's size on the substrate. In addition, the evaporation of the solvent also promotes precipitation of the drug out of solution, thus constituting a loss of efficiency as the drug then remains on the substrate instead of being atomized. When atomization does eventually occur, as seen by the rise in the curve at about 20 s, it is possible that this takes place when the remaining solvent is mainly octanol. In contrast, atomization is far better and appears immediately after power is applied for solutions dominated by octanol.

The time required for complete atomization of a fixed volume of the drug solution—the *atomization time*—is plotted in Fig. 9. This parameter was found to be controlled by the input power and the physical properties of the drug solution, especially the surface tension and viscosity. As expected, the atomization time increases with solution viscosity, the latter manipulated by the octanol/ethanol concentration ratio. However, the atomization time decreases as the applied power is increased due to stronger capillary destabilization and hence a greater number of interfacial jetting and break-up events. The effect of the solvent properties on the atomization time therefore becomes less important as the power is increased.

However, there is an operation trade-off. In order to obtain optimal droplet sizes below 5 μm for deep lung penetration and maximum drug delivery, larger octanol concentrations with higher viscosities and lower volatilities are favored. On the other hand, it is ideal that portable delivery devices administer a given volume of drug in the shortest possible time. This is facilitated by higher input powers where the effect of concentration on the atomization time is suppressed. An additional consideration here is that powers above 1.5 W lead to large drop deformation and hence the generation of unacceptably large 100 μm order droplets, as discussed in Sec. IIIA. Finally, thin fluid films desired for the formation of 1 μm order droplets are far more prone to evaporation than large aspect ratio drops. The complex relationships between these physicochemical processes and their effect on the atomization process make optimization of the device a challenge. Still, the results of our investigations provide some useful physical insight, confirmed by measurements with the lung model in the next section.

C. Dose measurements

Fig. 10 shows the various doses discussed in Sec. IID as well as the equilibrium flow rate as a function of the input power for the salbutamol/octanol system. Note that the equilibrium flow rate is controlled by the external syringe pump, which is adjusted to keep the volume of the liquid (*i.e.*, the parent drop volume) on the SAW device constant, and is hence not the true atomization rate because of evaporation and other losses. We first observe that the flow rate at equilibrium (curve 4) increases quite rapidly with increasing power, as expected given the larger energies delivered to the drop to drive interfacial destabilization and hence atomization, and consistent with our earlier observations.

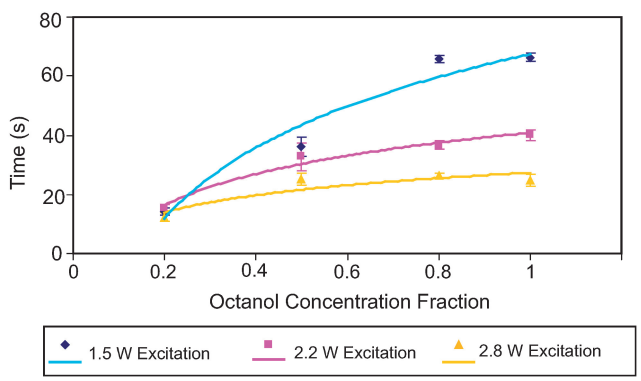

Fig. 9 Atomization time as a function of the octanol concentration fraction for different input powers. The trendlines are included to aid visualization.

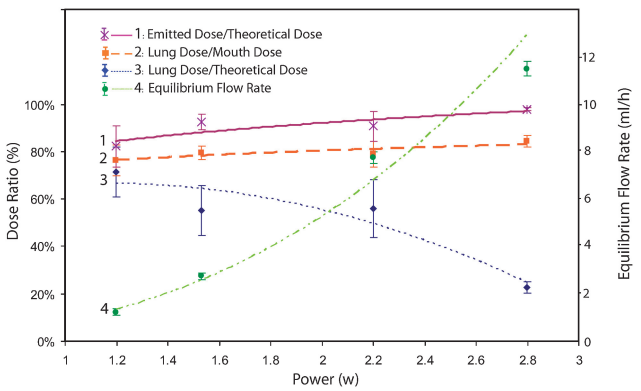

Fig. 10 Dose ratio and equilibrium flow rate as a function of power for the salbutamol/octanol system. The trendlines are included to aid visualization.

Consequently, the equilibrium flow rate must be greatly increased to maintain the parent drop volume. Further, Fig. 10 shows both the emitted to theoretical dose ratio (curve 1) and the lung to mouth dose ratio (curve 2) to increase with increasing input power, albeit weakly. Again, these observations are consistent with our aerosol characterization studies above.

With increasing power, the parent drop suffers from stronger deformations and hence generates a greater quantity of larger droplets within the 10 μm or even 100 μm order size range. Thus, the lung dose to emitted dose ratio (curve 3) decreases with increasing power. After trapping and collecting the large droplets that appear at the entrance of the impinger and deducting their volume from the emitted dose, we obtained the mouth dose. Thus, the lung dose increases with increasing power whereas the mouth dose decreases, as anticipated (curve 2). The emitted dose also increases compared to the theoretical dose since the atomization rate increases with increasing power, consistent with the increase in the equilibrium flow rate, thus delivering more of the drug off the surface into the aerosol in each period of time.

Recalling the definitions for the various doses in Sec. IID, it is therefore desirable to maximise the values of all dose ratios, *i.e.*, the emitted dose to theoretical dose ratio, the lung dose to mouth dose ratio, and the lung dose to the theoretical dose ratio, in order for the maximum amount of drug to reach the lower respiratory airway regions. These curves therefore suggest that the efficiency of the delivery increases, although only slightly (around 10%) with higher input power. In any case, the SAW drug delivery device is efficient, with more than 80% of the drug delivered into the respiratory system, as observed from curve 1. The remaining (<20%) drug loss is principally due to its precipitation on the device substrate. The lung dose is slightly lower, with a maximum close to 70% (curve 3), suggesting that only around 10% of the drug would be deposited in the upper respiratory tract (regions A and B).

On the other hand, the lung to theoretical dose ratio (curve 3) is observed to decrease sharply with increasing power. The competition between the gradual reduction of the average aerodynamic droplet diameter and the appearance of 100 μm order droplets from large-scale parent drop deformation (discussed in Sec. IIIA) as the power is increased is being won by the latter, sacrificing the lung to theoretical dose ratio: a small increase in emitted to theoretical and lung to mouth dose ratios (around 10%, curve 1) is far less than the drop in the lung to theoretical dose ratio (about 40%, curve 3). The device should therefore be operated at low to moderate powers, certainly under 1.5 W, such that the dose ratios across the various criteria are maximized.

In these cases of moderately low power atomization (~1.5–2 W), the atomization rate is around 2–4 ml h^{-1}, as suggested by curve 4. Since typically 0.1–0.2 mg of the drug is required per use, (*e.g.*, for Ventolin® and Buventol Easyhaler®), only 2–4 minutes for device operation is needed with a salbutamol concentration of 1 mg ml^{-1}. We note, however, that the atomization rate varies for different liquids.

The twin-stage lung deposition model employed here also provides preliminary data for a performance comparison with other devices. The lung to theoretical dose ratio, associated with the fraction of aerosols produced with sizes below 5.8 μm, is comparable with the cascade impaction data reported in other literature,[19] in particular, the respiratory deposition fraction for which aerosols under 5 μm are accounted. From the standpoint of dosage alone, the results here show that the SAW atomization technology is a strong competitor to other advanced nebulization designs which are currently on the market. For example, the ~80% lung to theoretical dose ratio and ~90% emitted dose to theoretical dose ratio is comparable to what is arguably regarded as the leading nebulizer on the market, Omron's Microair®, which has a respiratory deposition fraction of between 55 to 70% and an emitted dose fraction of around 90%.[19] The other advantages of SAW atomization, including its small size, low cost and low power requirement, together with its ease of use and potential for automation, then make the technology an attractive alternative to these conventional nebulizers.

IV. Conclusions

We have demonstrated that SAW atomization is a promising vehicle for generating suitable aerosol concentrations and size distributions for highly efficient inhaled pulmonary drug delivery. Although the investigations have been carried out on a single model drug, salbutamol, we believe the delivery platform itself is generic, implying that the device could be employed for the treatment of COPD, respiratory infections and other diseases where inhalation therapy may be effective. Moreover, its relative simplicity and low cost, low power requirements, portability, ease of use, silent operation and ability to nebulize aqueous solutions together suggest it is a viable and attractive alternative to conventional jet nebulization and other ultrasonic and electrohydrodynamic atomization techniques. It may even be configured to rival single dose devices such as MDIs. The potential for the system to atomize large molecule solutions without damage, for example, proteins such as insulin,[40] increase the potential usefulness of SAW atomization in clinical settings.

While further in-depth studies will be necessary, our preliminary investigations here on the characterization of the aerosol droplets, including some limited optimization of the device to increase its efficiency, already show the feasibility of the device to effectively and efficiently deliver aerosolized salbutamol solutions to regions deep in the lung.

The results indicate that the atomization process works best with lower volatility and higher viscosity solvents, in this case, octanol, at low to moderate input powers. Larger viscosities and lower powers tend to prevent the deformation of the parent drop, allowing the atomization to take place off a thin film and generally leading to the production of smaller aerosol droplets that fall within the 7 μm (slow breathing pattern), or 4.5 μm (rapid breathing pattern) cut-off aerodynamic diameters required for the droplets to be carried aerodynamically with the inhaled air flow through the highly bifurcated respiratory airways to the lower lung regions. Moreover, the lower volatility prevents the parent drop from evaporating and concomitant precipitation of the drug out of solution before atomization, thus maximizing the dose delivered by the device.

The low powers and higher viscosities, however, mean that the atomization rate is lower, prolonging the time required to atomize a given volume of drug solution. There is therefore a trade-off between increasing the lung dose (maximized by decreasing the droplet size through lowering the power and increasing the viscosity), quantified through the ratio of the lung

to mouth dose (curve 2 in Fig. 10), and increasing the delivery (or decreasing the total delivery time, which is optimized by increasing the power), quantified through the lung to theoretical dose (curve 3 in Fig. 10). Our studies, nevertheless, show that the increase in efficiency in the former is only slight with increases in power (around 10%), whereas the decrease in efficiency in the latter is significant (around 40%), suggesting that the optimum operating condition lies in the low to moderate power range below 1.5 W where both dose curves are relatively flat.

Even at these relatively low powers, which in itself is an advantage for potential miniaturization of the device, the lung to theoretical dose is high, around 70%, significantly larger than the 20–30% typically achieved with conventional nebulizers. These encouraging results provides support for SAW atomization as a viable microfluidic lab-on-a-chip platform for inhalation therapy and hopefully will inspire further work in this area.

References

1 R. B. Berry, R. A. Shinto, F. H. Wong, J. A. Despars and R. W. Light, *Chest*, 1989, **96**, 1241–1246.
2 H. Frijlink and A. Boer, *Exp. Op. Drug Del.*, 2004, **1**, 67–86.
3 B. H. J. Dickhoff, Ph.D. Thesis, University of Groningen, 2006.
4 A. R. Jada, M. Moher, G. P. Browman, L. Booker, C. Sigouin, M. Fuentes and R. Stevens, *BMJ*, 2000, **320**, 537–540.
5 D. E. Geller, *Resp. Care*, 2005, **50**, 1313–1322.
6 A. J. Hickey, ed., *Pharmaceutical Inhalation Aerosol Technology*, Marcel Dekker, New York, 2004.
7 L. Gradon and J. Marijnissen, eds., *Optimization of Aerosol Drug Delivery*, Kluwer, Dordrecht, 2003.
8 R. Dalbya and J. Suman, *Adv. Drug Del. Rev.*, 2003, **55**, 779–791.
9 R. Gregory, Ph.D. Thesis, Universite Catholique de Louvain, 2006.
10 N. Carroll, C. Cooke and A. James, *Eur. Resp. J.*, 1997, **10**, 292–300.
11 P. J. Barnes, *Curr. Op. Pharmacol.*, 2001, **1**, 217–222.
12 G. Scheuch, M. J. Kohlhaeufl, P. Brand and R. Siekmeier, *Adv. Drug Del. Rev.*, 2006, **58**, 996–1008.
13 M. Cloupeau and B. Prunet-Foch, *J. Aerosol Sci.*, 1994, **25**, 1021–1036.
14 J. Grace and J. Marijnissen, *J. Aerosol Sci.*, 1994, **25**, 1005–1019.
15 L. Y. Yeo, D. Lastochkin, S.-C. Wang and H.-C. Chang, *Phys. Rev. Lett.*, 2004, **92**, 133902.
16 D. A. LaVan, D. M. Lynn and R. Langer, *Nature Rev. Drug Disc.*, 2002, **1**, 77–84.
17 S. Z. Razzacki, P. K. Thwar, M. Yang, V. M. Ugaz and M. A. Burns, *Adv. Drug Del. Rev.*, 2004, **56**, 185–198.
18 R. Williams, *Drug Dev. Ind. Pharm.*, 2008, **34**, 913–922.
19 J. C. Waldrep and R. Dhand, *Curr. Drug Del.*, 2008, **5**, 114–119.
20 A. Qi, L. Y. Yeo and J. R. Friend, *Phys. Fluids*, 2008, **20**, 074103.
21 J. R. Friend, L. Y. Yeo, D. R. Arifin and A. Mechler, *Nanotechnology*, 2008, **19**, 145301.
22 M. Alvarez, J. R. Friend and L. Y. Yeo, *Nanotechnology*, 2008, **19**, 455103.
23 M. Alvarez, J. R. Friend and L. Y. Yeo, *Langmuir*, 2008, **24**, 10629–10632.
24 L. Y. Yeo and J. R. Friend, *Biomicrofluidics*, 2009, **3**, 012002.
25 K. Kulkarni, J. Friend, L. Yeo and P. Perlmutter, *Lab Chip*, 2009, **9**, 754–755.
26 D. Oxtoby, *Annu. Rev. Phys. Chem.*, 1981, **32**, 77–101.
27 International Commisssion on Radiological Protection, *Ann. ICRP*, 1994, **24**, 1–120.
28 H. Li, J. R. Friend and L. Y. Yeo, *Biomed. Microdev.*, 2007, **28**, 4098–4104.
29 M. K. Tan, J. R. Friend and L. Y. Yeo, *Lab Chip*, 2007, **7**, 618–625.
30 R. Shilton, M. K. Tan, L. Y. Yeo and J. R. Friend, *J. Appl. Phys.*, 2008, **104**, 014910.
31 H. Li, J. R. Friend and L. Y. Yeo, *Phys. Rev. Lett.*, 2008, **101**, 084502.
32 C. M. Sinton, B. I. Krosser, K. D. Walton and R. R. Llinas, *Eur. J. Physiol.*, 1989, **414**, 31–36.
33 N. E. Reich, B. A. Rosenberg and M. Metz, *Diseases Chest*, 1953, **22**, 43–49.
34 W. F. Miller, *Archives Int. Med.*, 1973, **131**, 148–155.
35 B. Marcet, F. Becq, C. Norez, P. Delmas and B. Verrier, *British J. Pharmacol.*, 2004, **141**, 905–914.
36 P. Kippax, *Pharma*, 2007, 46–49.
37 G. W. Hallworth and D. G. Westmoreland, *J. Pharm. Pharmacol.*, 1987, **39**, 966–972.
38 *British Pharmacopoeia*, 1999, Appendix XII F, p. A203.
39 C. M. Vozone and H. M. C. Marques, *J. Inclusion Phenom. Macrocyclic Chem.*, 2002, **44**, 111–115.
40 M. Alvarez, L. Y. Yeo, J. R. Friend and M. Jamriska, *Biomicrofluidics*, 2009, **3**, 014102.